PUBLICATIONS OF THE ASTRONOMICAL SOCIETY OF THE PACIFIC
103: 712–722, July 1991

EVALUATION OF SEEING ON A 62-CM MIRROR

M. IYE, T. NOGUCHI, Y. TORII, Y. MIKAMI, AND H. ANDO
National Astronomical Observatory, Mitaka, Tokyo 181, Japan

Received 1991 February 6, revised 1991 March 27

ABSTRACT

A 62-cm active optics telescope model with a Shack-Hartmann wavefront analyzer was used to measure the mirror seeing effect. The degradation of the imaging quality due to the generation of microthermal convection was quantitatively evaluated from diurnal monitoring measurements over 90 days and nights. The dependence of mirror seeing on the temperature difference between the mirror and the ambient air and the effect of flushing flow to blow away the microthermal turbulence were measured.

Key words: mirror seeing–convection–wind flushing–Shack-Hartmann camera

1. Introduction

The imaging quality of ground-based large telescopes is normally limited by the presence of wavefront aberration produced in the atmosphere. The degradation of the "seeing" takes place predominantly in the upper atmosphere, in the dome boundary layer, around the dome slit, in the telescope tube, and above the primary mirror surface. In order to maximize the imaging performance of costly large telescopes, the evaluation of the atmospheric seeing has been elaborately carried out recently to identify the best sites for these new telescopes. The effect of the boundary layer also has received attention to identify the best location on the site, the optimum height of the telescope above the ground, and the best shape of the dome. Significant design efforts have been made to reduce the effects of heat gained during the day and released during the night from the dome.

The effects of so-called mirror seeing were first quantitatively studied by Lowne 1979, who used a Schlieren camera to measure the mirror seeing for a 25-cm mirror. He found that the seeing degradation is roughly proportional to the temperature difference between the mirror and the ambient air and that the rate of degradation is about 0″.5/° C. His measurement, however, covered the temperature difference larger than 2° C and smaller than 8° C. To study the effect of mirror seeing on high-resolution imaging, more accurate measurements are definitely necessary especially for situations with smaller temperature difference. Barr et al. 1990 have recently given the results of their careful experiments to measure the mirror seeing for a 1.8-m mirror placed in a closed, unheated mirror-polishing facility. They evaluated the effect of flushing wind that passes over the mirror to reduce the mirror seeing degradation for a number of cases with controlled mirror-to-air temperature differences ranging between −2° C and 2° C. They found that no mirror seeing could be detected in the temperature difference range between −0.5° C and 0.5° C, but the effects became increasingly large for larger temperature difference. Flushing did reduce the seeing degradation due to the mirror, at least momentarily, until the air layer above the flushing flow got disturbed by returning flow.

The present paper reports the results of our extensive attempts to evaluate the seeing degradation observed in a 62-cm engineering telescope built originally for an active optics experiment.

2. Seeing Monitoring Setup

The actual setup used for the present experiment is shown in Figure 1. The basic telescope system was originally designed to verify the technical feasibility of the active optics concept (Iye 1989; Iye et al. 1990). The primary mirror was a 62-cm diameter Pyrex glass mirror of spherical meniscus shape with 2.1-cm thickness and 300-cm radius of curvature. The mirror was supported both axially and radially by nine prototype actuators developed for the Japan National Large Telescope (JNLT) and at three fixed points. The supporting forces at these 12 points were continuously monitored by high-precision load cells. A Shack-Hartmann wavefront analyzer with an internal light source was located at the center of curvature of the mirror (Noguchi et al. 1989). A CCD camera, electrically cooled to − 18° C, was used as the detector of the wavefront analyzer to measure the distribution of about 300 spots produced by a microlens array which was placed at the exit pupil of the telescope. The centroids of these spots were measured to an accuracy of 0.05 pixel by means of bisectioning to evaluate the wavefront aberration.

The control computers were used to adjust the support-

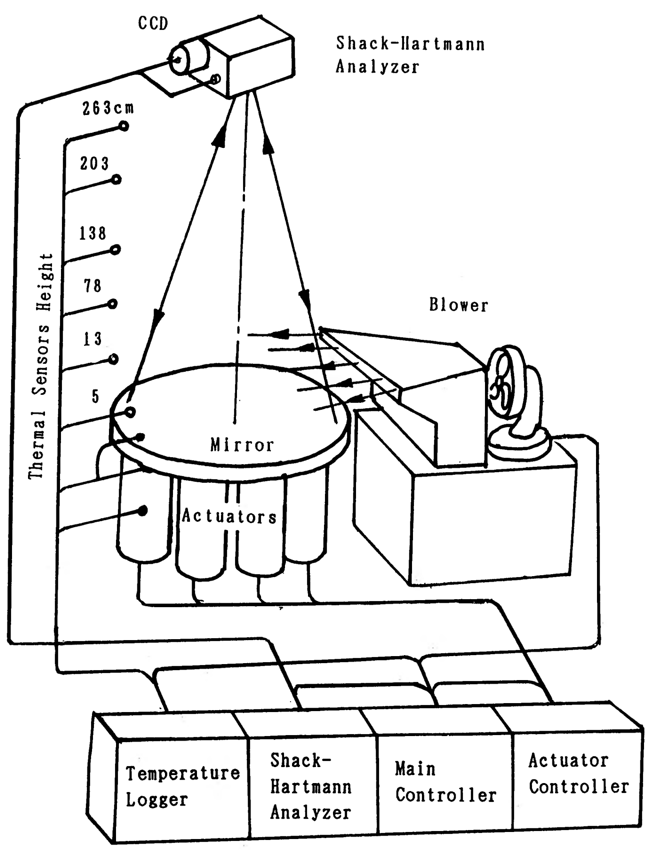

FIG. 1–Layout of the mirror seeing evaluation experiments.

ing forces of the nine actuators either by an open-loop mode or by a closed-loop mode. The supporting force distribution was kept to the prescribed values in the open-loop mode. On the other hand, the force distribution was adjusted in the closed-loop mode to compensate for the figure error of the mirror surface measured by the wavefront analyzer. The telescope system can be tilted to any elevation angle. The details of this basic setup and the essential results of the original experiments were reported in Iye et al. 1990.

Equipments added to this basic system to carry out the present experiments were a set of 20 temperature sensors, an electric fan with a flow-guide nozzle, and wind-velocity sensor. In the present experiments, the main personal computer controlled three dedicated computers which monitored and controlled the Shack-Hartmann camera, the actuators, and the temperature sensors. The telescope was pointed toward the zenith throughout the present experiments. The entire system was located in an 8-m-high laboratory built for testing balloon-borne telescopes on the Mitaka campus.

3. Measurements

3.1 *Temperature Monitoring*

The present experiments were designed to monitor the change of the wavefront aberration continuously over 24 hours under the natural diurnal cycle of temperature variation. No active attempt was made to control the thermal environment of the laboratory except for the contiguous on-off operation of an electric fan to blow away the turbulence, which naturally helped to mix the air in the laboratory. The number of measurements is therefore very large, amounting to about 60,000 measurements of aberrations in 81 runs over 90 full days. This enabled us to attain improved statistical significance in the measured results.

The temperature distribution was monitored by 20 calibrated bead thermistors with 0°01 C resolution. The air temperature was measured at the opposite sides of the telescope truss at six levels: 5, 13, 78, 138, 203, and 263 cm above the mirror. The temperature of the structure was also monitored at one point on the front surface and at two points on the back surface of the mirror, at three metallic actuators, and at two points on the telescope truss. The layout of the thermistors is also shown in Figure 1.

3.2 *Zernike Expansion*

The wavefront aberration $z(r,\theta)$ measured by the Shack-Hartmann analyzer was expanded by a complete orthogonal set of Zernike polynomials as

$$z(r,\theta) = \sum_{n=2}^{\infty} A_n^0 R_n^0(r) + \sum_{n=1}^{\infty} \sum_{m=1}^{n} (A_n^m \cos m\theta + B_n^m \sin m\theta) R_n^m(r) \ , \quad (1)$$

where $R_n^m(r)$ are the radial functions of the Zernike circle polynomials, A_n^m and B_n^m are the expansion coefficients for $U_n^m = R_n^m(r) \cos m\theta$ and $U_n^{-m} = R_n^m(r) \sin m\theta$, respectively, with $n - m$ being even.

The number of modes actually used in the Zernike expansion, N_z, should in principle be infinite. In practice, however, we have taken $N_z = 27$, including all the modes A_n^m and B_n^m with $1 \leq n \leq 6$ and $0 \leq m \leq n$, except for the trivial mode with $n = m = 0$.

As a global measure to represent the imaging quality under the presence of seeing degradation, we use the Strehl number S defined by

$$S = 1 - 2\pi^2 \, \mathrm{STR}^2/\lambda^2 \ , \quad (2)$$

where STR^2 is given by

$$\mathrm{STR}^2 = \sum_{n=2}^{\infty} \{2(A_n^0)^2/(n+1)\} + \sum_{n=1}^{\infty} \sum_{m=1}^{n} [\{(A_n^m)^2 + (B_n^m)^2\}/(n+1)] \ . \quad (3)$$

In addition to this "raw" Strehl number, denoted S_{raw} hereafter, we use "intrinsic" Strehl number S_{int}, in which the contribution from the image displacement components A_1^1, B_1^1, and A_2^0 are removed. The intrinsic Strehl number $S_{\rm int}$ is therefore defined by an expression similar to equation (2) where STR^2 is replaced by

$$STR^2_{\rm int} = \sum_{n=4}^{\infty} \{2(A_n^0)^2/(n+1)\} + \sum_{n=2}^{\infty} \sum_{m=1}^{n} [\{(A_n^m)^2+(B_n^m)^2\}/(n+1)] \ . \qquad (4)$$

The raw Strehl number $S_{\rm raw}$ gives a measure to evaluate the central intensity of the point-spread function normalized to that for the diffraction-limited image. The intrinsic Strehl number $S_{\rm int}$ gives the corresponding measure to evaluate the central intensity when the wavefront aberration of tilt terms A_1^1, B_1^1, and the defocus term A_2^0 are removed by means of a fast image stabilizer and an autofocuser. Considering the wavelength response of the CCD chip, we assume that the effective wavelength λ of measurement was about 700 nm.

It should be noted that equation (2) gives an approximate expression to evaluate the Strehl ratio and that the values derived from equation (2) depart from the actual Strehl ratio, giving lower values, especially when the phase error is large. We discuss, however, only the relative changes of $S_{\rm raw}$ and $S_{\rm int}$ under various conditions and will not deal with the absolute values in this paper. The usage of the approximate expression (eq. (2)) for the Strehl ratio should, therefore, be adequate.

3.3 *Mode of Measurement*

A wind-flow guiding nozzle with an outlet 70 cm wide and 2 cm high and a 40-cm square inlet was placed in front of an electric fan to generate a laminar flushing wind flow. The effect of flushing wind to blow away the microturbulence was evaluated by measuring the difference of wavefront aberrations with the fan turned on and turned off.

Continuous monitoring of the wavefront aberration allowed us to evaluate the generation of microturbulence under an unstable thermal stratification. For a typical run, the Shack-Hartmann measurement was continuously carried out at 2-minute intervals for 24 hours. The electric fan was turned on and off at 4-minute intervals to allow comparison of wavefront aberration with and without flushing flow alternatively. The timing to start exposure was set to ensure that the flushing flow produced by a fan becomes a steady stable flow. The electric fan was turned off as soon as the exposure was finished.

Three parameters, i.e., the exposure time, the height of the blower, and the power of the blower, define the mode of measuring runs. The summary of measuring runs in various modes is given in Table 1.

TABLE 1
Number of Runs of Measurements

Blower Voltage	Blower Height	Exposure time 3 sec	10 sec	30 sec	Total
100 V	13 cm	8	8	5	21
	33 cm	5	3	3	11
	60 cm	4	4	4	12
	88 cm	4	2	2	8
60 V	13 cm	4		5	9
	33 cm	2			2
	60 cm	6			6
40 V	13 cm	4	4	4	12
Total		37	21	23	81

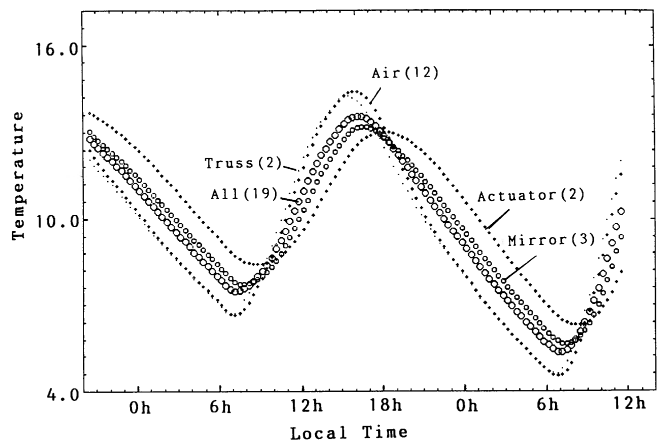

FIG. 2–Diurnal variation of mean temperature of the air, the mirror, the actuator, and the telescope truss. The number of sampling points to derive the mean temperature is shown in parentheses. The variation of all the sampling points is also shown for reference. Note the presence of time lag in the temperature variations of the mirror and of the actuator with respect to that of the air.

4. Measuring Temperature and Flushing Wind

4.1 *Diurnal Temperature Variation*

Figure 2 shows a typical example of the diurnal variation of mean temperatures of the air, the glass mirror, the metallic actuator, and the metallic truss. The variation of the temperature of the mirror and the actuators shows significant time delay of the order of a few hours with respect to that of the ambient air because of their large thermal inertia. Such a diurnal cycle of temperature variation produces a temperature difference between the mirror and the ambient air. Due to this time lag, the mirror is generally warmer than the air during the night and cooler than the air during the daytime. The temperature difference is larger on clear days and smaller on cloudy or rainy days.

Figure 3 shows a typical example of the diurnal variation of the air temperature measured at six levels above the mirror surface. The air temperature at 5 cm and at 13 cm above the mirror showed smaller amplitude of diurnal variation as compared with those at higher levels. This is partly due to the structure of the telescope center section of the present setup which prevented air circulation and

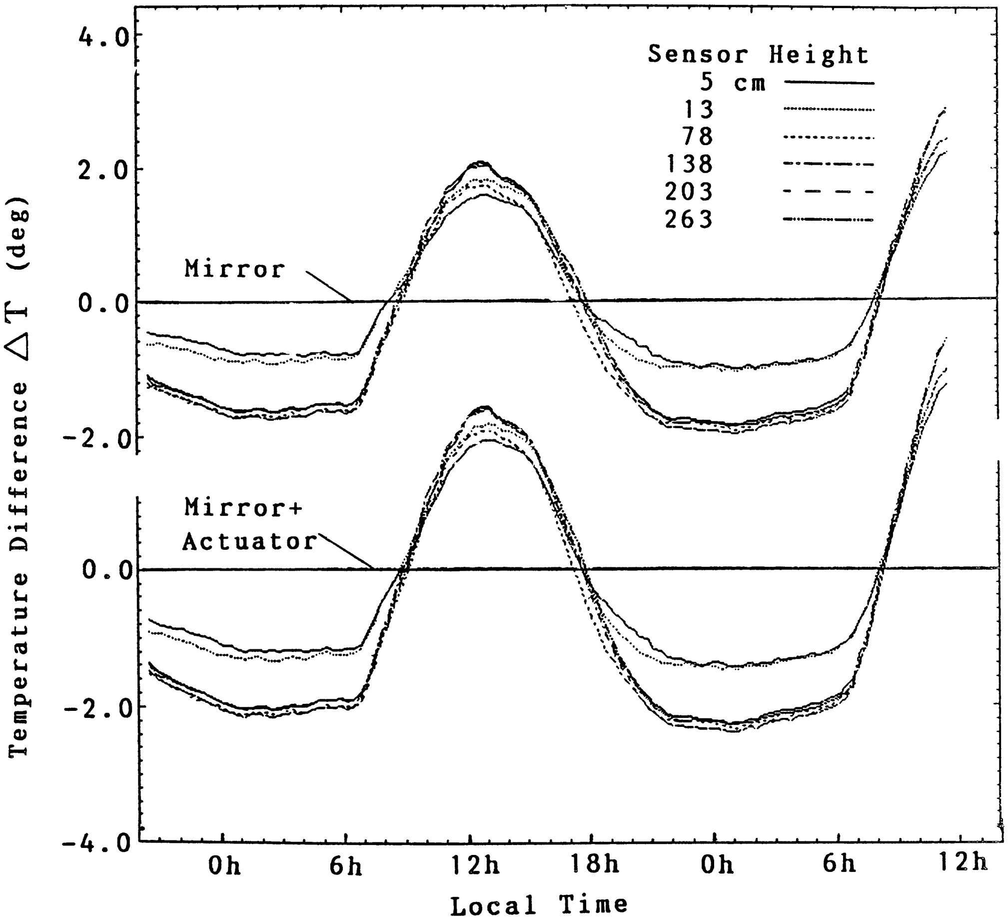

FIG. 3–Diurnal variation of the temperature deviation of the air with respect to that of the mirror, ΔT. The air temperature was sampled at various heights above the mirror surface. The upper panel shows the temperature deviation of the air with respect to the mirror temperature, while the lower panel shows that with respect to the mean temperature of the mirror and the actuator.

enhanced radiative heat exchange with the air. The trapped air is cooled down during the night but not as much as the air above the center section, because the mirror surface is generally warmer than the air during the night.

The upper panel of Figure 3 takes the mirror temperature as the reference temperature, whereas the lower panel takes the average temperature of the mirror and the metallic actuators, to define the temperature difference. Since the thermal inertia is much larger for the mirror-actuator assembly than for the mirror itself, the time delay between the variations of the air temperature and the material temperature is also larger for the latter case. The derived values of the temperature difference, therefore, show larger amplitude of diurnal variation.

4.2 *Temperature Profile*

Figure 4 gives a normalized vertical profile of the nighttime air temperature averaged over 90 nights. The mirror temperature was used for reference to calibrate the time variation. Significant change of mean temperature is observed near the mirror surface. The vertical temperature profile for the stable stratification, where the mirror is cooler than the air, is not exactly symmetric to that for the unstable case, where the mirror is warmer than the air. In the case of unstable stratification, the Brunt-Vaisala frequency described in a later section is evaluated from the measured temperature profile. The convectively unstable zone appears to reach up to 15 cm above the mirror surface.

4.3 *Wind-Velocity Profiles*

Figure 5 shows the measured profiles of flushing wind flow. The vertical thickness of the flushing flow was about 10 cm at the mirror center (Fig. 5c). The wind velocity was fairly uniform along the transverse direction of the flow as shown in the transverse profile measured over the mirror center at the height of the flow center (Fig. 5b). The wind-velocity profile along the stream shows a slight increase and a subsequent drop instead of a steady decrease downward (Fig. 5a). This is probably because the measurement for this profile was not carried out exactly at the height corresponding to the center of the flow. Unfortunately, the wind-velocity measurement along the flow

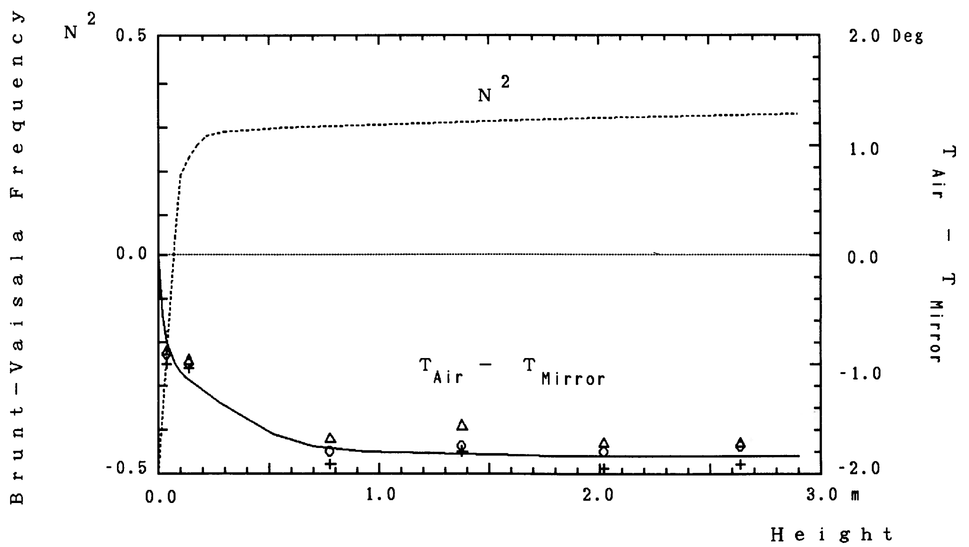

FIG. 4–Mean vertical profile of the nighttime air temperature. The mirror temperature was used for reference to calibrate the time variation. The Brunt-Vaisala frequency N^2 calculated from this vertical temperature profile is also shown.

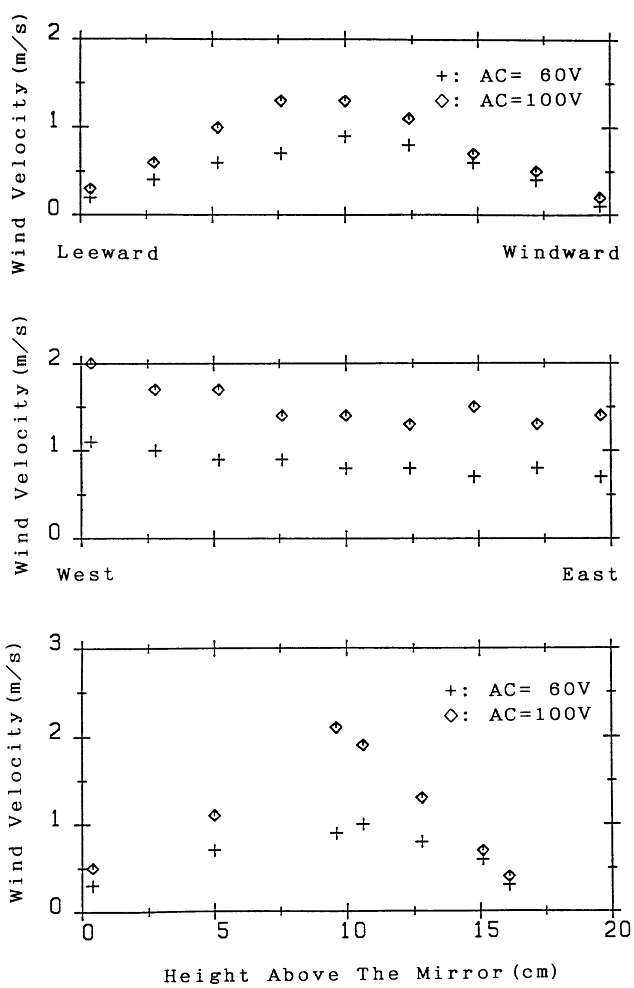

FIG. 5–Wind-velocity profiles: (a) profile along the flow, (b) transverse profile, and (c) vertical profile.

was carried out only at this height during the entire runs and we have no additional data to confirm this.

5. Zernike Coefficients

5.1 *Diurnal Variation*

Figure 6 shows an example of the diurnal variation of temperature, dispersion of the Zernike coefficients for astigmatism A_2^2, and the Strehl numbers S_{raw} and S_{int} measured over 36 hours. Since the drift in temperature caused slow but long-term variation of Zernike coefficients, the dispersions from the running mean of five consecutive measurements over 20 minutes were evaluated for each Zernike coefficient to represent the fluctuating components.

It is noted that the astigmatism and the Strehl numbers show larger dispersion during the night than during the daytime. The period showing larger dispersion precisely coincides with the period when the mirror is warmer than the ambient air. This fact strongly indicates that microturbulence is generated from the warmer mirror surface. The long-term slow variation of lower-order aberrations can be ascribed mainly to the thermal drift of the mechanical structure and partly to the real change in the air stratification. We assume that the deviation of aberrations from their corresponding running means is entirely due to air turbulence and call them the contribution from the mirror seeing. Microturbulence arising from the warm mirror can be effectively removed by flushing wind flow as will be shown in Figure 7.

5.2 *Flushing Effect*

Figure 7 shows the Strehl intensities plotted against the temperature difference between the mirror and the air $\Delta T (= T_{mir} - T_{air})$. When the flushing flow was not applied, the degradation of the Strehl intensity is

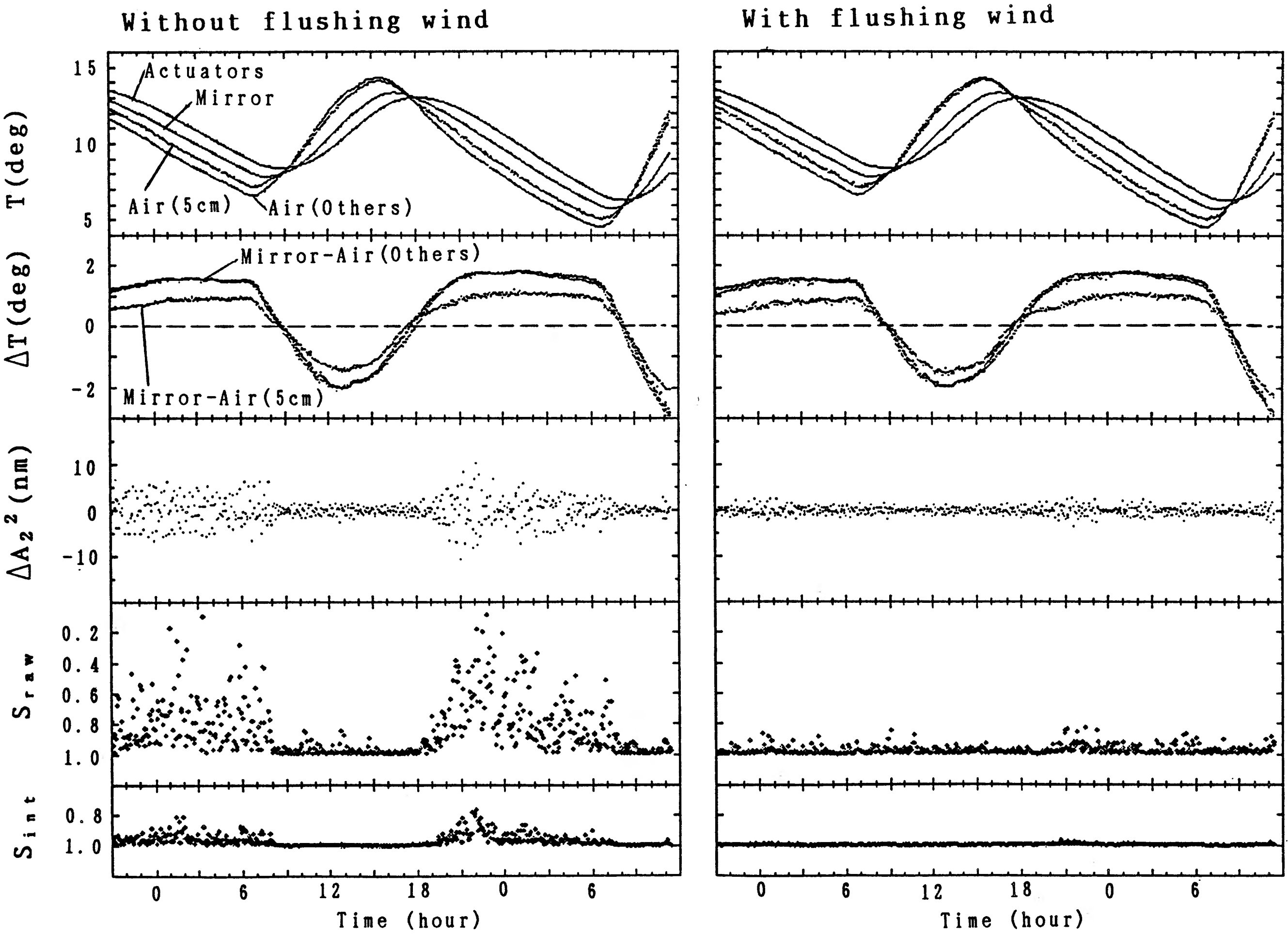

FIG. 6–Diurnal variation of the temperature T, temperature difference between the mirror and the air ΔT, Zernike coefficients for astigmatism A_2^2, and the Strehl numbers S_{raw} and S_{int}.

observed as is shown in the upper-left panel for temperature difference $\Delta T > 0$. This can be interpreted as the generation of convective bubbles rising from the mirror surface, which perturb the wavefront. The exposure time for each measurement was 3 sec. The measured values therefore correspond to the time-averaged wavefront. Since the motion of the convective bubbles is predominantly vertical, the time average in this case can be interpreted as the "vertical" average.

The amount of degradation appears significantly reduced by turning on the fan to generate flushing wind flow as is shown in the upper-right panel. Since the flushing flow transports the convective bubbles horizontally, the time average here may be interpreted as the "horizontal" average. Flushing flow of 1 m sec^{-1} conveys bubbles well across the mirror surface during a 3-sec exposure time. Comparison of the upper-left and upper-right panels indicates that the "horizontal" average is more effective than the "vertical" average in reducing the wavefront perturbation. This is a plausible result if one considers the columnar structure of the convective layer.

Comparison of upper panels for S_{raw} and lower panels for S_{int} in Figure 7 shows that the contributions from wavefront tilt and defocus terms are very large. This result indicates the importance of developing and utilizing a fast autoguider and an autofocuser for observations that require high angular resolution.

5.3. *Exposure Time*

Figure 8 shows the effect of different exposure time to measure the aberration. Due to the limitation of the light source, exposure time was set to 3, 10, and 30 sec to assure high-enough S/N to allow bisectioning of the spot images. The intensity of the light source was adjusted to give constant S/N ratio independent of the exposure time. Naturally, the values of the Strehl numbers defined in the present paper increase as the integration time increases from 3 sec to 30 sec, since the contributions from the short-term variation of the seeing are averaged out in long-exposure measurements. The shortest time constant of actual atmospheric seeing variation can be as small as 2 msec (Roddier, Northcott & Graves 1991). Mirror seeing

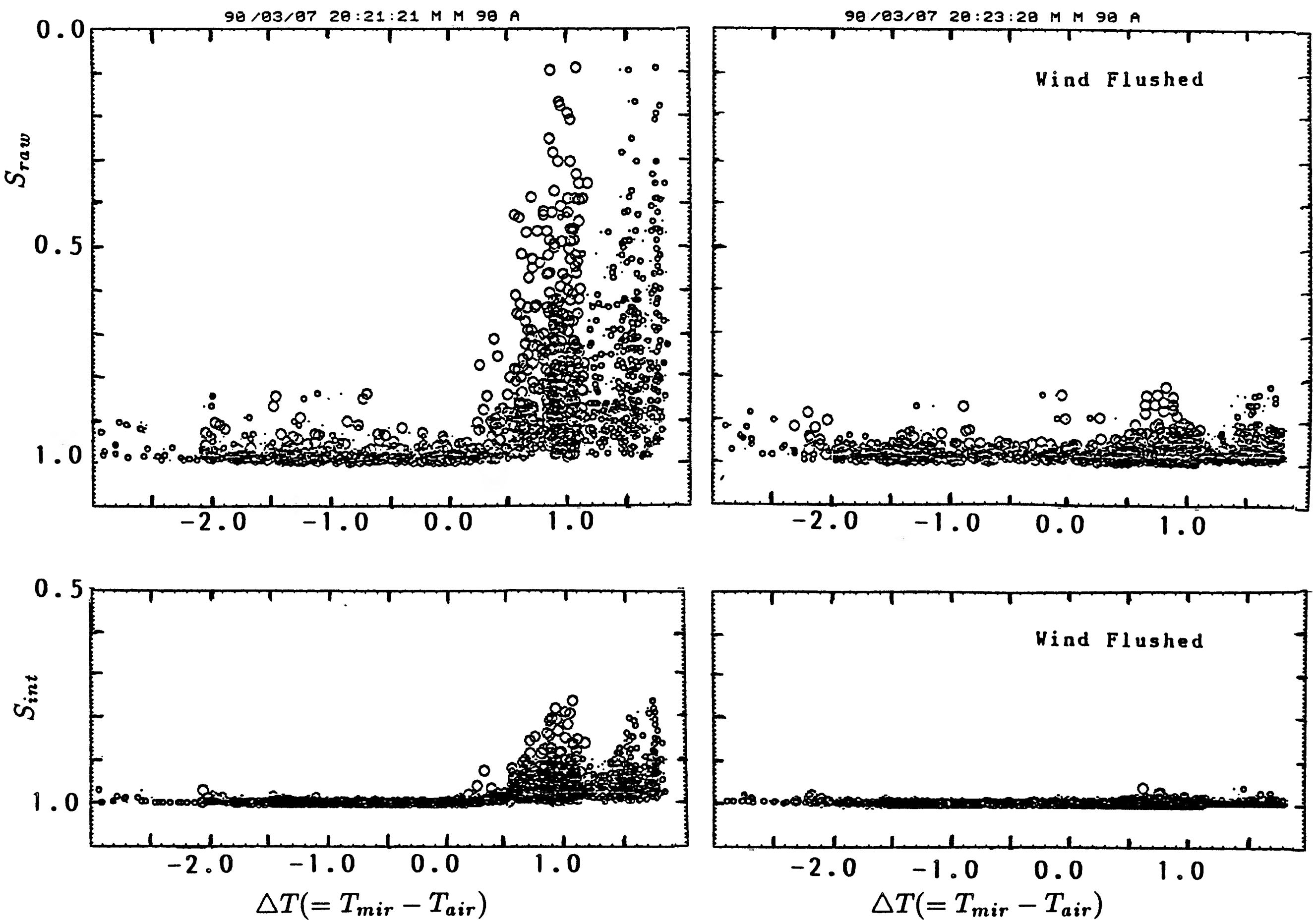

FIG. 7–Strehl intensities S_{raw} and S_{int} versus temperature difference between the mirror and the air, ΔT, showing the generation of mirror seeing (left panels) and the effect of flushing flow to remove the mirror seeing (right panels).

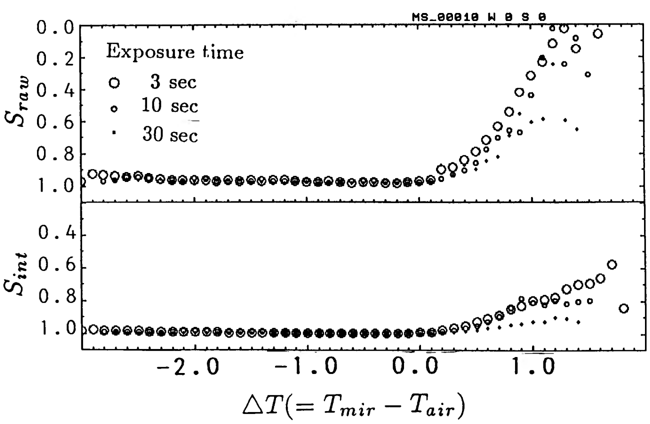

FIG. 8–Mean Strehl intensities S_{raw} and S_{int} versus temperature difference ΔT at various exposure times, showing the averaging effect.

measurements by Barr et al. 1990 showed the presence of turbulence at 1-millisec exposure. Therefore, the actual image degradation due to the seeing effect would be larger than the value measured in the present experiment.

Barr et al. 1990 showed by comparing the interferograms taken at 1-millisec exposure that the flushing flow helps in reducing the turbulence attributable to a warm mirror even at such a short time scale.

5.4 *Evaluation of the Temperature Difference*

In order to evaluate the effects of flushing flow speed and of the flushing flow height under various temperature conditions, many 24-hour runs of measurement were carried out on clear days and cloudy days for each category of setup parameters.

The temperature difference between the mirror and the air was measured using three different definitions. ΔT_1 is the difference between the mean of the mirror temperature sampled at two points on the backside of the glass mirror and the mean of the air temperature sampled at two points at 5 cm above the mirror surface. ΔT_2 is defined as the difference between the mean temperature of the mirror sampled at three points (one at the front surface and two at the back surface) and the mean air temperature sampled at two points at 5 cm above the mirror surface. ΔT_3 is the difference of the mean temperature of the mirror at three points and the mean air temperature sampled at 12 points as was shown in Figure 1.

Since the backside of the glass mirror is exchanging heat with the massive actuators, the amplitude of the diurnal temperature variation is even smaller than that of the front surface of the mirror. There is therefore a relation such that $|\Delta T_1| < |\Delta T_2| < |\Delta T_3|$.

Figure 9 shows the Strehl numbers S_{raw} and S_{int} versus temperature differences ΔT_1, ΔT_2, and ΔT_3 for measurements with the flushing flow turned off extracted from 37 short-exposure runs. The Strehl number shows the similar dependence on the three indices of the temperature difference. However, it should be noted that the image degradation coefficients as derived from the gradient of the right side of the curves in Figure 9 are quantitatively different according to the definition of the temperature difference. We shall use the index ΔT_1 hereafter unless otherwise noted.

If we accept seeing degradation so far as $S_{int} > 0.8$, it is necessary to maintain the temperature difference between the mirror and the air just above the mirror in the range $\Delta T < 1°$ C.

5.5 *Flushing Efficiency*

The efficiency of the flushing flow is evaluated by a normalized efficiency introduced by Barr et al. 1990. The normalized efficiency of the flushing flow to improve the imaging quality is defined by

$$E = \{(S_{int})_{on} - (S_{int})_{off}\}/(S_{int})_{off} \ , \qquad (5)$$

where $(S_{int})_{on}$ and $(S_{int})_{off}$ are the measured intrinsic Strehl number with and without flushing flow. The flushing is effective for improving the imaging quality when the flushing efficiency $E > 0$. On the other hand, the flushing can deteriorate the imaging quality when $E < 0$.

5.6 *Height of the Flushing Flow*

Since the upper edge of the center section of the telescope truss structure was at about 10 cm above the mirror, it prevented direct flushing of the air just above the mirror surface. The actual height of the flushing flow was set either at 13 cm, 33 cm, 60 cm, or 88 cm.

Figure 10 shows the normalized flushing efficiency E versus the temperature difference $\Delta T(= T_{mir} - T_{air})$ between the mirror and the air. The air temperature was measured at 13 cm above the mirror for these experiments and the data for three blower levels above the mirror are shown. The data for a blower height of 60 cm are omitted in this diagram, since they fall between those for 33 cm and for 88 cm . The wind velocity was set to 1 m $\sec^{-1}$, and the exposure time was 3 sec for the upper panel and 30 sec for the lower panel.

The flushing efficiency was positive in a convectively unstable situation, $\Delta T > 0$. Namely, in convectively unstable cases where the mirror is warmer than the air, the flushing flow can remove convective bubbles and contribute to improve the image quality. Although the amount of degradation due to the generation of convection and the resulting amount of improvement by flushing flow are small near the convectively neutral situation with $\Delta T = 0$, the present measurement with much improved accuracy has shown that the onset of convection takes place at $\Delta T = \Delta T_0$, where $0 < \Delta T_0 < 0.2$ C.

Barr et al. 1990 confirmed the presence of mirror seeing for $\Delta T > 0.5$ C. Although the definitions of ΔT are different between the present experiment and that carried out by Barr et al., it is likely that mild convection

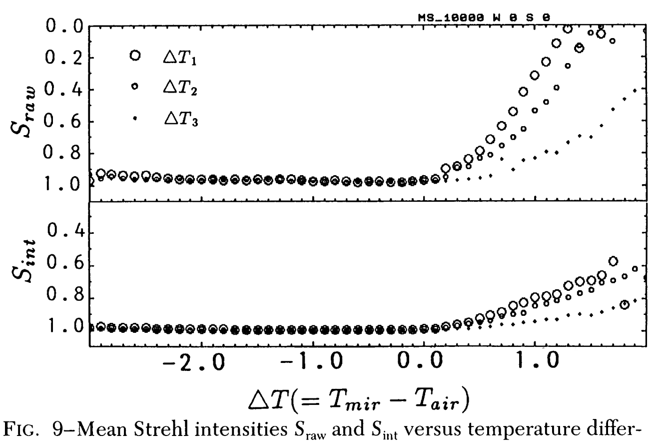

FIG. 9–Mean Strehl intensities S_{raw} and S_{int} versus temperature difference ΔT for three definitions.

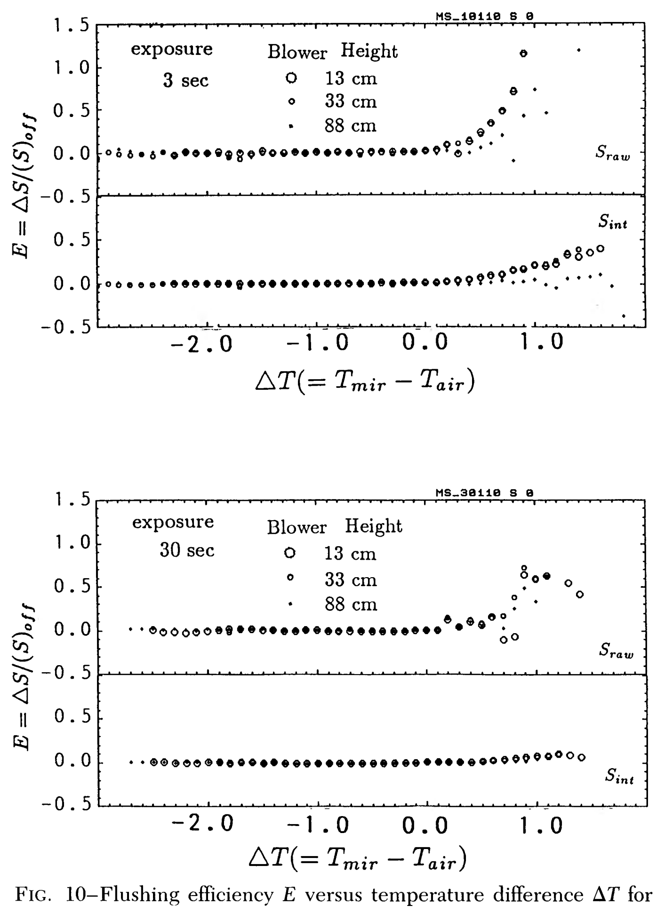

FIG. 10–Flushing efficiency E versus temperature difference ΔT for measurements with three different blower heights, showing the effectiveness of flushing flow near the mirror surface. Flushing efficiency is calculated from S_{raw} and S_{int} for short-exposure runs (upper panel) and for long-exposure runs (lower panel).

is actually generated even at situations with 0° C < ΔT < 0°.5 C.

Figure 10 shows that the flushing efficiency is positive and is larger for flushing flow blown closer to the mirror surface. Namely, the flushing is effective in reducing degradation of the image when blown at heights of 13 cm and 33 cm but not so much at 88 cm.

If the mixing length, or the turnover length, of rising bubbles is long enough, we expect that the height of the flushing flow plays an important role. Namely, by assuming that the air layer below the flushing height is turbulent while the layer above that can be kept undisturbed, we expect naturally better seeing by setting flushing flow at a height closer to the mirror surface. Flushing flow helps to prevent convective bubbles rising far up into the optical path.

If the mixing length of convective bubbles is relatively short, flushing flow above the convective zone will not contribute to reducing the aberration. The main role of the flushing flow in the convective zone to reduce the aberration will be the "horizontal" averaging effect as was described before. Anyway, Figure 10 appears to be consistent with these expectations.

It would be worth noting that in convectively stable cases where the mirror is cooler than the air by $\Delta T <$ $-2°$ C, the image can be slightly degraded if the flushing flow is turned on. Namely, the flushing efficiency becomes slightly negative as is barely seen in Figures 10 and 11. This phenomenon can be interpreted as the excitation of turbulence, and possibly a gravity wave as well, by the flushing flow in the stable air stratification, as will be discussed in Section 6.

5.7 *Wind Velocity*

The driving voltage of the electric fan was set at 100 V, 60 V, and 40 V during the present experiment. The wind velocity measured by a wind-velocity sensor of bridge resistor type with velocity resolution of 0.05 m sec^{-1} was 1.0 m sec^{-1}, 0.5 m sec^{-1}, and 0.2 m sec^{-1}, respectively, for 100 V, 60 V, and 40 V.

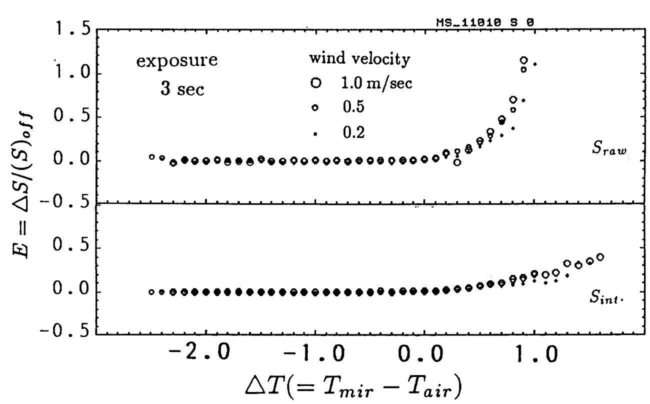

FIG. 11–Flushing efficiency E versus temperature difference ΔT evaluated at various flushing wind velocities. Flushing efficiency was evaluated from S_{raw} and from S_{int} for runs with a short-exposure time of 3 sec.

Figure 11 shows the flushing efficiency E versus temperature difference ΔT at different wind velocities. Although there is a tendency that stronger wind provides larger flushing efficiency, the difference is not very significant. This means that even a mild flushing flow can contribute to removing the convective bubbles. This result, however, will depend on the size of the mirror and the time resolution of the measurement.

6. Analysis

6.1 *Convection*

The Rayleigh number R defined by

$$R = -\alpha\, T\, d^4 N^2/\kappa\nu \quad , \tag{6}$$

should be used to characterize the convective motion. Here, α, κ, ν, d, and N denote, respectively, the expansion coefficient, thermal-conduction coefficient, viscosity, thickness of the convective layer, and the Brunt-Vaisala frequency, as given in equation (7). There is a certain critical Rayleigh number R_c beyond which ($R > R_c$) the convective motion actually sets in.

Instead of using the Rayleigh number, we use here the Brunt-Vaisala frequency introduced in the mixing-length theory and make rough estimations on the thickness of the thermal convective zone, the velocity of the convective bubbles, and their turnover time. The expression for the Brunt-Vaisala frequency, which is used as a criterion to predict the convective instability ($N^2 < 0$), is

$$N^2 = g\{(d\ln T/dh)_{ad} - (d\ln T/dh)\} = (g/c_p - \delta T/\delta L)g/T \quad , \tag{7}$$

where c_p and g denote the specific heat at constant pressure and the gravitational acceleration, respectively, and δT denotes the temperature difference over a vertical scale of δL.

The vertical profile of N^2 evaluated from the measured temperature profile is shown in Figure 4, which suggests that the air stratification up to about 7 cm above the mirror surface is convectively unstable. In practice, convective bubbles will overshoot up to 2–3 times the thickness of the unstable zone. We therefore assume that the convection zone typically has a thickness of about 20 cm or so in the present experiment. It is interesting to relate this value with the efficiency of the flushing flow at various heights (cf. Fig. 10). Namely, the fact that the flushing efficiency was large for runs with the blower set at 13 cm and also at 33 cm above the mirror but not so much for runs with the blower set at 88 cm appears compatible with the present estimation of the depth of the convective zone.

The mean velocity of the convective bubbles can be evaluated by the following equation:

$$v^2 = (dT/dh - g/c_p)Lg/\sqrt{2}T \quad , \tag{8}$$

where L is the mixing length and dT/dh is the temperature gradient. Assuming $L = 7$ cm and evaluating dT/dh at the midlevel of the convection zone in Figure 4, we obtain a velocity of about $v = 2$ cm sec^{-1} and a turnover time for a bubble of about 15 sec.

The acceleration in convective motion is proportional to the superadiabatic gradient $|dT/dz - (dT/dz)_{ad}|$, which is generally much smaller than the actual temperature gradient $|dT/dz|$ for the present experiment. Hence, the temperature difference δT over the height difference δL gives an acceleration due to the buoyancy of $\alpha = kg$, where the reduction factor k is of the order $k = 0.001$.

6.2 *Gravity Wave Oscillation*

The flushing efficiency as calculated for S_{raw} became slightly negative when the electric fan was turned on for cases with a convectively stable air stratification with $\Delta T < -2°$ C. Although the amount of degradation is small, it was observed not only for runs with an exposure time of 3 sec but also for runs with 30-sec exposure (cf. Figs. 10 and 11). The degradation was not confirmed for the range $-2°$ C $< \Delta T < 0°$ C. No corresponding degradation was confirmed for S_{int}.

The generation of turbulence by the flushing flow is a natural explanation for this. It is, however, noted that the degradation was not significantly reduced by increasing the exposure time, suggesting the presence of a long-period component in this phenomenon. The fact that degradation can be seen only for S_{raw} and not for S_{int} suggests that the long-wavelength components, if any, were excited.

Another possibility is the excitation of gravity oscillation of the air in the building. Although rigorous analysis taking the boundary conditions into account is beyond the scope of the present paper, a simple consideration is given here. The frequency of the internal gravity oscillation in a stable case can also be given by the Brunt-Vaisala frequency N. The frequency of this oscillation at 1 m, for example, above the mirror surface gives the oscillation period $P = 2\pi/N$ of about 11 sec. This corresponds roughly to the oscillation period of a gravity wave with a wavelength corresponding to the horizontal size of the cavity of the building. Whether the long-period component likely observed for runs with stable air stratification is due to the generation of turbulence or due to the excitation of gravity wave oscillation by the flushing fan requires further study.

7. Conclusion

Some remarks should be made before summarizing the conclusions of the present experiments. First of all, as was mentioned before, the present measurement used an integration time equal to or longer than 3 sec due to purely technical reasons. The measured amount of image degradation due to microturbulences will, therefore, be smaller than the actual values. On the other hand, the approximate expression of equation (2) for the Strehl ratio gives somewhat overestimated values of the image degradation. Second, a light source placed at the center of curvature of the mirror was used to evaluate the mirror seeing. The region along the telescope tube where the wavefront aberration is measured is therefore essentially a conic region with the prime focus as an apex of the cone, instead of a cylindrical region which the light from stars passes through. Third, the measurement was done in a closed laboratory without active ventilation.

Despite these limitations, we summarize the conclusions of the present experiments as follows.

(1) The wavefront perturbation due to the convection generated by a warm mirror was quantitatively measured by means of a Shack-Hartmann camera. About 60,000 measurements were carried out under various conditions over 90 days and nights to evaluate the quantitative characteristics of mirror seeing with a high statistical accuracy.

(2) The mirror-seeing degradation was confirmed to be present when the mirror is warmer than the ambient air. Since the mirror and its support mechanism have larger thermal inertia than the surrounding air, the temperature of the mirror does not fall immediately in response to the temperature drop of the ambient air during the night. Therefore, the degradation due to the mirror seeing generally takes place during the night.

(3) The temperature inversion generates convective bubbles. Due to the high accuracy attained in the present measurements, the deterioration of the Strehl numbers due to the mirror seeing was confirmed to be present for $\Delta T (= T_{mir} - T_{air}) > 0.2°$ C.

(4) These bubbles, however, can be flushed away by means of a laminar wind flow generated over the mirror surface. Wind flushing is proved to be useful to improve imaging quality under the presence of degradation due to mirror seeing. A laminar flushing flow should be generated and guided to pass over the mirror as close as possible to the surface.

(5) The wavefront tilt terms were identified among others to play the major role for the mirror seeing.

(6) Theory of convection was used to estimate the thickness of the convective zone, the velocity of the convective bubble, and the circulation time. Convective bubbles are found to rise up to about 20 cm above the mirror surface for the present setup.

(7) Slight degradation of the Strehl number S_{raw} was observed by turning on the flushing flow when the air is in a stable stratification with $\Delta T < -2°$ C. This is partly due to the generation of turbulence which mixes the cool part of the air below the flow with the warm part above the flow. Possible excitation of long-period gravity wave oscillation of the air in a building cavity is also remarked.

(8) The present experiments indicate the importance of controlling the mirror temperature to satisfy the condi-

tion $\Delta T < 1° C$ and installing a wind-flushing capability for any costly large telescope to reduce the degradation of image quality due to the generation of mirror seeing.

The authors are grateful especially to Profs. Y. Yamashita and F. Roddier and Dr. L. Barr for their helpful comments on the original manuscript.

REFERENCES

Barr, L. D., Fox, J., Poczulp, G. A., & Roddier, C. A. 1990, SPIE, 1236, 492
Iye, M. 1989, Ap&SS, 160, 149
Iye, M., Noguchi, T., Torii, Y., Mikami, Y., Yamashita, Y., Tanaka, W., Tabata, M., & Itoh, N. 1990, SPIE Proc., 1236, 929
Lowne, C. M. 1979, MNRAS, 188, 249
Noguchi, T., et al. 1989, Pub. National Astr. Obs. Japan, Vol. 1, 49
Roddier, F., Northcott, M., & Graves, B. 1991, PASP, 103, 131